A Theoretical Analysis of Low-Frequency Sonophoresis: Dependence of Transdermal Transport Pathways on Frequency and Energy Density

Ahmet Tezel,[1] Ashley Sens,[2] and Samir Mitragotri,[1,3]

Received August 19, 2002; accepted September 9, 2002

Purpose. Application of low-frequency ultrasound has been shown to increase skin permeability, thereby facilitating delivery of macromolecules (low-frequency sonophoresis). In this study, we seek to determine the dependence of transport pathways during low-frequency sonophoresis on ultrasound parameters.

Methods. Pig skin is exposed to low-frequency ultrasound over a range of frequencies to achieve different skin resistivities. The porous pathway model is used to study the dependence of average pore size, porosity, and tortuosity on ultrasound parameters. Imaging experiments are also carried out to visualize the transport pathways created by ultrasound.

Results. The data show that the average pore size, determined from the porous pathway model, does not depend on application frequency. Both in the presence and absence of ultrasound the average pore size determined from mannitol delivery is the same (28 ± 12 Å). With the application of ultrasound the skin porosity could be increased by up to 1700-fold. The effect of ultrasound on skin is heterogeneous thereby creating localized transport pathways (LTP). The porosity of these transport pathways is of the same order of magnitude as that of the dermis.

Conclusions. With this study it is shown that low-frequency ultrasound increases skin permeability by increasing skin porosity rather than by increasing the size of the pores that are responsible for permeant delivery.

KEY WORDS: sonophoresis; porous pathway; porosity; skin; permeability.

INTRODUCTION

Transdermal drug delivery (TDD) offers an advantageous alternative to common delivery methods such as injections or oral delivery. However, applications of transdermal delivery are limited by low skin permeability. Specifically, stratum corneum (SC), the outermost layer of the skin, provides an outstanding barrier against the external environment and is responsible for skin's barrier properties (1–3). SC is a relatively thin (10–15 μm) impermeable membrane that consists of flat, dead cells that are filled with keratin fibers (corneocytes) surrounded by lipid bilayers (3,4). The highly ordered structure of lipid bilayers confers upon the SC an impermeable character. Different techniques, such as chemical enhancers (3,5,6), iontophoresis (7), electroporation (8), and ultrasound (sonophoresis) applied at both therapeutic (1–3 MHz) (9) and low frequency (20–100 kHz) (10) conditions have been used to enhance transdermal drug transport.

Low-frequency sonophoresis (LFS) is significantly more potent in enhancing skin permeability compared to therapeutic sonophoresis (*f*~1–3 MHz) (11). This is a direct consequence of increased acoustic cavitation (formation, growth, and collapse of gas bubbles) at low ultrasound frequencies (12). LFS has been shown to increase transdermal drug delivery rates of hydrophilic solutes that usually posses low permeabilities under passive conditions (11). We showed earlier that transdermal transport due to LFS depends on two parameters; the ultrasound frequency and energy density (13). Tang *et al.* have shown that transdermal transport of hydrophilic permeants in both the absence and presence of LFS can be described using a porous pathway model (14). Li *et al.* have also shown that the porous pathway model adequately describes iontophoretic delivery of mannitol (15). This model is an explicit, commonly used physical model which assumes that tortuous cylindrical channels of constant cross sectional area are responsible for permeant delivery across a membrane. Although the model adequately describes transdermal transport of hydrophilic solutes, the existence of these pores within the skin has still not been confirmed experimentally. Our rationale for the existence of pores is as follows: Due to the low permeability of lipid bilayers to highly hydrophilic solutes, transdermal transport of such solutes is unlikely to occur through intact intercellular lipid bilayers. We propose that transdermal transport of such solutes may take place through defects (imperfections) that could occur between/within the lipid lamellar organization. Such defects are known to occur naturally within the highly ordered structure of lipid bilayers (16,17). Porous pathway model describes diffusion of a hydrophilic solute through these defects. In that case, solute transport is determined by the pore size, porosity and tortuosity. In this study we advance our understanding of the pathways through which ultrasound enhances skin permeability to hydrophilic solutes. Specifically, using the porous pathway model, we studied the dependence of pore size, porosity, and tortuosity on ultrasound frequency (20 kHz – 100 kHz) and energy density (0–2000 J/cm^2).

MODEL SUMMARY

The fundamental underlying assumption of the porous pathway model is that both in the absence and presence of ultrasound, hydrophilic permeants migrate through the skin via tortuous cylindrical pores. As noted above we do not propose that these pores are geometrically distinct and identifiable structures but rather imperfections in the lipid bilayers. Other model assumptions include: (i) the permeants/ions behave as hard spheres that have no specific interactions with the pore walls and (ii) the anions and cations in the electrolyte solution have the same valance, z, and similar diffusion coefficients. In this study sodium and chlorine ions are the two dominant current carrying ions in the electrolyte solution, thereby satisfying the second assumption. Later a brief description of the model is given. A detailed description of the porous pathways could be found in literature (14,18).

The general expression for permeability, P_p of a hydrophilic permeant diffusing through a porous membrane (e.g. skin) is given by:

[1] Department of Chemical Engineering, University of California Santa Barbara, Santa Barbara, California 93106.

[2] Department of Chemistry, Santa Barbara City College, Santa Barbara, California 93109.

[3] To whom correspondence should be addressed. (e-mail: samir@engineering.ucsb.edu)

0724-8741/02/1200-1841/0

$$P_p = \frac{\varepsilon D_p^{pore}}{\tau \Delta x} \quad (1)$$

where ε, τ, and Δx are the porosity, tortuosity, and thickness of the membrane, respectively, and D_p^{pore} is the diffusion coefficient of the permeant in the liquid-filled pores within the membrane. According to the hindered transport theory (18), D_p^{pore} is a function of both the permeant and the membrane characteristics. D_p^{pore} can be expressed as a product of the permeant diffusion coefficient at infinite dilution, D_p^{∞}, and permeant diffusion hindrance factor, $H(\lambda_p)$, where λ_p is the ratio of the hydrodynamic radius of the permeant, r_p, and the average pore radius of the membrane, r, i.e., $\lambda_p = r_p/r$. With the aforementioned changes Eq. (1) becomes as follows:

$$P_p = \frac{\varepsilon}{\tau \Delta x} D_p^{\infty} H(\lambda_p) \quad (2)$$

For λ_p<0.4, the diffusion hindrance factor, $H(\lambda_p)$, is given by the following (18):

$$H(\lambda_p) = (1 - \lambda_p)^2 (1 - 2.104\lambda_p + 2.09\lambda_p^3 - 0.95\lambda_p^5) \quad (3)$$

An equation similar to Eq. (2) can be written for the permeability of current carrying ions. Specifically,

$$P_{ion} = \frac{\varepsilon}{\tau \Delta x} D_{ion}^{\infty} H(\lambda_{ion}) \quad (4)$$

where D_{ion}^{∞} is the ion diffusion coefficient at infinite dilution, and $H(\lambda_{ion})$ is the hindrance factor for the ion, given by Eq. (3) with λ_p replaced by λ_{ion}, where $\lambda_{ion} = r_{ion}/r$, with r_{ion} the hydrodynamic radius of the ion. Combining Eqs. (2) and (4) gives:

$$\frac{P_p}{P_{ion}} = \frac{D_p^{\infty} H(\lambda_p)}{D_{ion}^{\infty} H(\lambda_{ion})} \quad (5)$$

By relating P_{ion} to skin resistivity and D_{ion}^{∞} to electrochemical properties of PBS, Tang *et al.* have shown that Eq. (5) can be rewritten as follows:

$$log\ P_p = log\ C_3 - log\ R \quad (6)$$

where R is the skin resistivity ($k\Omega \cdot cm^2$) and C_3 is:

$$C_3 = \frac{kT}{2z^2 F c_{ion} e_0} \frac{D_p^{\infty} H(\lambda_p)}{D_{ion}^{\infty} H(\lambda_{ion})} \quad (7)$$

where k is the Boltzmann constant (1.38×10^{-23} J/K/molecule), T is the absolute temperature (298 K), z is the electrolyte valance (1), F is the Faraday constant (9.648×10^4 C/mol), c_{ion} is the electrolyte molar concentration (0.137 M) and e_0 is the electronic charge (1.6×10^{-19} C). Eq. (6) indicates that a plot of $log\ P_p$ vs. $log\ R$ should exhibit a linear behavior with a slope of –1. Eq. (6) provides a general equation to theoretically describe the diffusion of a hydrophilic permeant across the skin under any permeation conditions, including passive control and diffusion after ultrasound treatment. However the y-intercept ($log\ C_3$) may differ for the various permeation conditions, depending on the average pore radius, r, corresponding to a particular permeation condition. Accordingly, a change in r manifests itself through a change in the intercept of $log\ P_p - log\ R$ correlation, whereas changes in ε, τ, and Δx do not affect the intercept value. Once the pore size is determined ε/τ can be determined from the following two equations.

$$\frac{\varepsilon}{\tau} = \frac{\Delta x}{\sigma_{sol} R} \frac{1}{H(\lambda_{ion})} \quad (8)$$

or

$$\frac{\varepsilon}{\tau} = \frac{\Delta x P_p}{D_p^{\infty} H(\lambda_p)} \quad (9)$$

where σ_{sol} is the conductivity of the electrolyte solution.

The primary objective of this study is to understand the nature (e.g. size) of the transdermal transport pathways (r, ε/τ) created by LFS. We have previously shown that the enhancement induced by LFS (in the range of 20 kHz–100 kHz) depends on the ultrasound frequency and the energy density, (i.e., E, where energy density is the product of ultrasound intensity, I, and application time, t) (13). Hence, the pathways created by LFS are also likely to depend on ultrasound frequency and energy density. In the following sections the dependence of ε/τ, $H(\lambda_{ion})$, and Δx on the frequency and energy density will be investigated.

MATERIALS AND METHODS

In vitro Experiments

In vitro experiments were carried out with full–thickness pig skin (Yorkshire). The animal was euthanized using pentobarbital (100 mg/kg). Skin on the back and the lateral flank was harvested immediately after sacrificing the animal. The underlying fat was removed and the skin (i.e., dermis and epidermis) was cut into small pieces (2.5 cm × 15 cm). Skin pieces with no visible imperfections such as scratches and abrasions were wrapped in aluminum foil and stored in a –80°C freezer to be used over a period of 12 weeks. Before each experiment the skin was thawed at room temperature and was mounted on to a Franz diffusion cell (Permegear, Hellertown, PA). Only skin having an initial resistivity of 30 $k\Omega \cdot cm^2$ or more was used to ensure that the skin was intact. Methods for conductivity measurement are described later.

A Franz diffusion cell consists of a donor and a receiver compartment. A 4-mm Ag/AgCl disk electrode (In vivo Metrics, Healdsburg, CA) was introduced in both compartments for skin conductivity measurements during the experiment. The receiver compartment was filled with a sodium/potassium phosphate buffered saline (PBS) (Sigma–Aldrich, St. Louis, MO). The solution has a phosphate concentration of 0.01 M and NaCl concentration of 0.137 M. PBS was prepared using deionized water with ~8 MΩ-cm resistivity. A magnetic stirrer bar was added to the receiver compartment. The donor compartment was filled with a solution of Sodium Lauryl Sulfate (SLS), (1% weight/volume) in PBS. SLS (Sigma–Aldrich, St. Louis, MO) was chosen as the model surfactant because its effect on transdermal transport in the presence of ultrasound has been relatively well characterized (19,20). The diffusion cell was placed in a custom-made plexi-glass mounting block. The solution in the receiver compartment was stirred with a magnetic stirrer (Bell Stir, Vineland, N.J.). Ultrasound was applied using the methods that will be described in the next section. All experiments were carried out at room temperature.

Following the ultrasound application the SLS solution in the donor compartment was replaced with a solution of radiolabeled mannitol (ARC, St. Louis, MO) in PBS (5 μCi/ml). The receiver compartment was stirred at a speed of 400 rpm throughout the experiment. Samples from the receiver compartment were withdrawn at predetermined time points, and the concentration of the permeant in both donor and receiver compartments (C_d and C_r, respectively) were measured using a scintillation counter (Packard, Meriden, CT). Skin permeability, P_p, to a given permeant, was calculated as follows:

$$P_p = \frac{1}{A\Delta C}\frac{dQ}{dt} \tag{10}$$

where ΔC is the permeant concentration difference between the donor and the receiver compartments, A (2.2 cm^2) is the permeation area, and Q is the cumulative amount of permeant transported into the receiver compartment at time t at steady state.

Ultrasound Application

Four custom built transducers with operating frequencies of 19, 58, 76 and 93 kHz (Piezo Systems, Cambridge, MA) were used for application of ultrasound. The transducers were designed by sandwiching ceramic crystals between two metal resonators of appropriate lengths (6.1 cm, 6.1 cm, 4.6 cm, 3.6 cm respectively for 19 kHz, 58 kHz, 76 kHz and 93 kHz). The cross sectional area of all transducers was 0.785 cm^2. A signal generator (Tektronix CFG-280, Beaverton, OR) along with an amplifier (Krohn–Hite 7500, Avon, MA) was used to drive the transducers. The electric power applied to the transducer was measured using a sampling wattmeter (Clarke–Hess 2330, New York, NY). The frequency of the electrical signal was matched with the resonant frequency of each transducer. An inductor was connected in parallel with each transducer to optimize its performance. The values of the inductors were 10.06 H, 1230 mH, 682 mH, and 472 mH respectively for 19 kHz, 58 kHz, 76 kHz, and 93 kHz. The transducer was placed at a distance of 3 mm from the skin in the donor compartment. A 100% duty cycle and an acoustic intensity, I, of 1.08 W/cm^2 was chosen for ultrasound application. We showed earlier that the enhancement is a direct function of the total ultrasound energy density, E (E = intensity x total application time), although this function depends on frequency (Fig. 1) (13). At any frequency a desired skin permeability could be reached regardless of the intensity if the application time is varied (13). A typical temperature increase of <10°C, was observed in 2 min when ultrasound was applied. For this reason, the donor solution (i.e., the coupling medium) was changed every two minutes during the experiment by turning off the ultrasound. Control experiments were carried out to assess the effect of temperature on skin conductivity. No significant enhancement of skin conductivity was observed when the skin temperature was increased/decreased by 10°C without ultrasound.

Electrical Resistance Measurements

The skin conductivity was measured at the end of sonication. The presence of skin between the donor and receiver compartments introduces an additional resistance (in series) to the already present resistance of PBS. The resistance of the skin was calculated by applying a 143-mV AC voltage at 10Hz (Agilent 33120A, Palo Alto, CA) and measuring the current. The same procedure was repeated without mounting the skin. The difference between these two values is the resistance of the skin itself. The skin resistance was then multiplied with the skin area (2.2 cm^2) to calculate the skin resistivity. Skin conductivity is the reciprocal of skin resistivity.

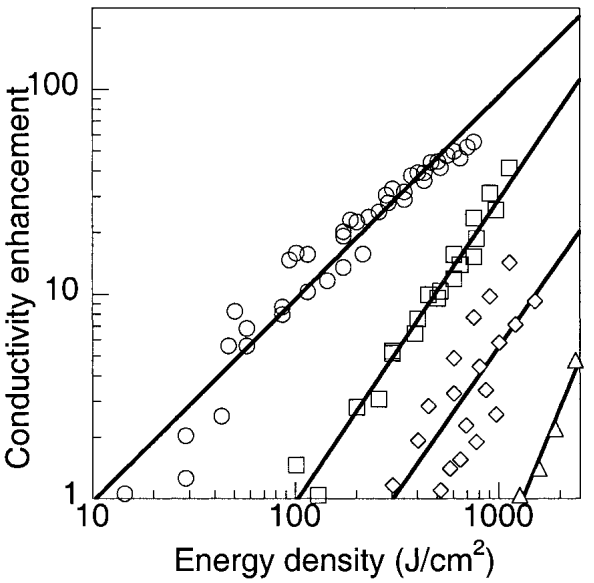

Fig. 1. The skin conductivity enhancement as a function of energy density for four frequencies ((○)-19 kHz (□)-58 kHz, (◇)-76 kHz, (△)-93 kHz). The lines correspond to power fits to the data (r^2 = 0.97, 0.97, 0.71, 0.99 for 19 kHz, 58 kHz, 76 kHz, 93 kHz, respectively). Each point represents an average of 6–8 experiments.

Imaging of Transport Regions in the Stratum Corneum

Sulforhodamine B (SRB) (Molecular Probes, Eugene, OR) was used for visualizing the transport regions in the SC. Skin was exposed to the SRB/SLS solution along with ultrasound using the methods discussed above. Skin was then removed from the diffusion cell, rinsed and was imaged using a digital camera (Optronics, Goleta, CA). Although SRB is a fluorescent dye it was used as a colorimetric dye. The dye was used at concentrations in the range of 1 mM–5 mM. The elapsed time between the removal of the skin from the diffusion cell and imaging was less than 15 min. No diffusion of SRB patches was apparent during this time. The fractional area of the transport regions with respect to the total sonicated area was quantified using Adobe Photoshop. The cross sectional depth of SRB delivery was also measured by cutting the skin vertically at the transport pathways. The depth of delivery was also quantified by Adobe Photoshop.

RESULTS AND DISCUSSION

Dependence of Average Pore Size on Ultrasound Parameters

Earlier we reported the dependence of skin conductivity (*1/R*) on ultrasound frequency and energy density (13). For any value of enhancement, there exists an energy density (regardless of frequency) that can be used to achieve the desired

conductivity enhancement, although the required energy density increases substantially with ultrasound frequency (Fig. 1). This result suggests that with LFS, the effect of two parameters, ultrasound frequency and energy density could be lumped into one parameter; the skin resistivity. To study the dependence of pore size on ultrasound parameters, the skin was sonicated at each frequency (19 kHz, 58 kHz, 76 kHz, and 93 kHz) in separate experiments in the presence of 1% SLS until a set skin resistivity was reached. The steady state permeability was measured in each experiment. At each frequency, mannitol permeability was measured for skins possessing resistivity values between 70 kΩ.cm^2 and 0.5 kΩ.cm^2. Energy densities to reach these conditions at each frequency are shown in Fig. 1. Figure 2 shows the *log* P_p vs. *log R* graph for all four frequencies studied. The intercept values (i.e., *log* C_3) and the average pore radii were calculated from Eq. 7 for each case in Table I. Because the intercepts for all four frequencies are not statistically different ($p < 0.05$), it could be concluded that ultrasound frequency does not affect the average pore radius as determined from mannitol permeability (28 ± 12 Å). Because the passive diffusion experiments show the same trend (Fig. 2) as shown by LFS experiments, average pore radius for passive diffusion is also 28 Å. Li *et al.* also reported that for iontophoretic delivery of mannitol, the size of pores induced by iontophoresis was comparable to that of preexisting pores for passive diffusion (15).

If the passive delivery of hydrophilic permeants is hypothesized to occur through the defects (imperfections) in the skin, then LFS could be generating more of these already existing imperfections. In such case the average pore radius will not be altered with different frequencies because ultrasound does not create different (unique) types of pathways. The conclusion that pore size of sonicated skin is not altered compared to passive diffusion is consistent with data reported by Tang *et al.* (14). Because the average pore size is unaffected by ultrasound application, i.e., $H(\lambda_p) \approx$ constant, the increased skin permeability of hydrophilic permeants due to ultrasound must be explained by increased porosity and/or decreased tortuosity. The ε/τ ratio for each permeability condition can be calculated by both Eqs. (8) and (9). In the next section the choice for the membrane thickness, Δx, will be discussed because this value is required for the calculation of the ε/τ.

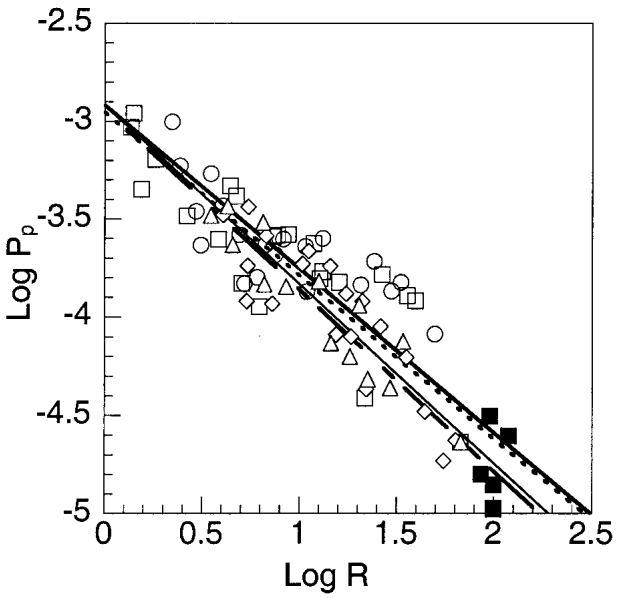

Fig. 2. log P_p – log R graph ((○)-19 kHz (□)-58 kHz, (◇)-76 kHz, (△)-93 kHz, (■)-passive diffusion). The lines correspond to linear fits to the data (r^2 = 0.91, 0.91, 0.93, 0.96 for 19 kHz, 58 kHz, 76 kHz, 93 kHz, respectively). The intercept values are –2.92, –2.91, –2.92, –2.94 for 19 kHz, 58 kHz, 76 kHz, 93 kHz, respectively.

Table I. Intercept, i.e. log C_3, Values and the Corresponding Average Pore Radii for All Four Frequencies

Frequency (kHz)	log C_3 Mannitol	Pore radius mannitol (r) Å
19	–2.92 ± 0.048	28 ± 10
58	–2.91 ± 0.047	29 ± 9
76	–2.92 ± 0.056	28 ± 12
93	–2.94 ± 0.049	26 ± 8

Note: pore radius, *r,* for all cases was calculated using Eq. (7). The error ranges on the pore radius were determined using the error on the intercept values.

The Dependence of Δx on Ultrasound Parameters

For passive delivery of permeants through the skin, the SC is responsible for skin barrier properties. In this case, Δx (membrane thickness) would be the SC thickness (15 μm). However, with the application of LFS this assumption needs reconsideration. Specifically, the effects of ultrasound on skin are heterogeneous, creating localized transport pathways (LTP) (13,20). Figure 3 shows LTPs created with the application of ultrasound in the presence of SLS and Sulforhodamine B, a colorimetric dye. Also, in Fig. 4A, the cross sectional depth of SRB delivered at LTPs is presented. During LFS, solutes are assumed to traverse the skin only through LTPs. After the solute traverses through a distance $\triangle x$ and exits the LTP, 100% of the skin area is available for diffusion. Our calculations show that, regardless of skin permeability, diffusion through the LTP is the rate-limiting step in determining skin permeability. Because increasing permeability of the skin usually corresponds to increased LTP depth, it also results in a longer diffusion path length. We hypothesize that because the LTP depth during LFS is significantly higher than the SC thickness, the SC is no longer the main barrier for permeant delivery. With the application of ultrasound, as the

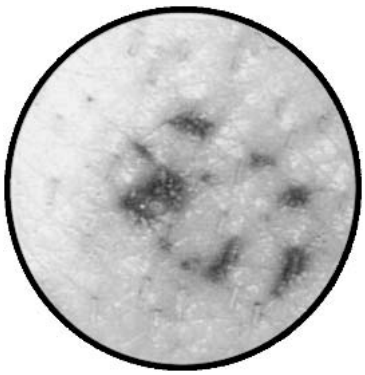

Fig. 3. Generation of LTPs after application of low-frequency ultrasound at 58 kHz (intensity = 1.08 W/cm^2) with SLS in the presence of SRB. LTPs correspond to dark spots.

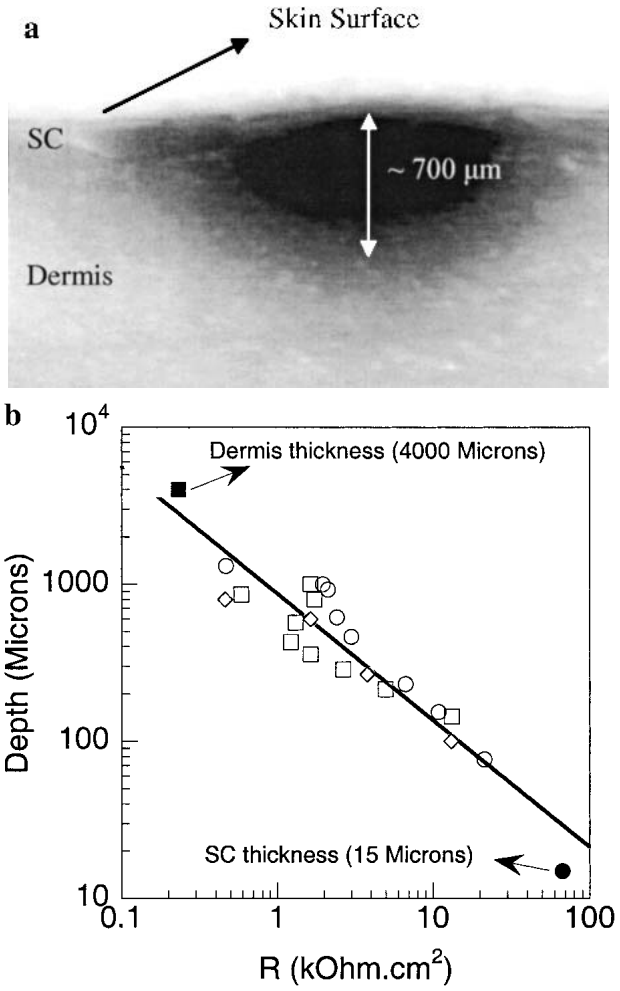

Fig. 4. (a) The cross sectional depth of SRB delivery with ultrasound at 58 kHz (intensity = 1.08 W/cm^2). (b) the cross sectional depth of SRB delivery as a function of skin resistivity for three frequencies ((○)-19 kHz (□)-58 kHz, (◇)-76 kHz). The upper and lower limits of depth of transport pathways, that the dermis and SC thickness, are also shown (■)-dermis, (●)-SC).

SC permeability increases, the next rate-limiting barrier for permeant delivery would be the epidermis followed by the dermis. The permeability within the LTP is the effective permeability of the SC + epidermis + dermis region. Within these three regions SC is the least permeable region followed by the epidermis. Permeabilities for SC and epidermis within the LTP are ~10^{-4} and ~10^{-3} cm/hr, respectively (estimated using data from Fig. 2). We hypothesize that because the permeability values of the SC and epidermis sections are much lower than the effective LTP permeability (2.0×10^{-2} cm/hr), the dermis in the LTP possession higher permeability values than the intact dermis (1.0×10^{-2} cm/hr). In view of the higher permeability of the LTP compared to unaffected SC in area even in the dermis, LTPs dominate the transdermal transport even in the dermis.

The dermis permeability was measured by isolating the dermis from the SC and epidermis using heat stripping. Because a separate analysis of ε/τ values within the SC, epidermis, and dermis is not feasible we assumed that the average ε/τ value within the total affected depth could be calculated. Experiments were carried out to study the dependence of the LTP depth as a function of skin resistivity. In these experiments ultrasound was applied until particular skin resistivity values were reached (in the range 100 kΩ.cm^2–0.5 kΩ.cm^2) then the skin was cut along the LTP and the depth of penetration of SRB was measured for each case. In Fig. 4B, the penetration depth is plotted as a function of and skin resistivity. Fig. 4B shows that the cross sectional depth of the LTPs is a function of skin resistivity (resistivities of dermis and SC are also shown for reference). However, there is no frequency dependence ($p < 0.05$). Note that the effective membrane thickness is set at the end of ultrasound application and does not depend on "mannitol permeation time". In other words, a steady state in physical structure is reached at the end of ultrasound application before the skin is contacted with mannitol. Also, without ultrasound no visible penetration of the dye occurs if the skin (full thickness or heat stripped) is contacted with the dye for 10 min. To calculate ε/τ values a data fit was applied in Fig. 4B to represent Δx as a function of skin resistivity, R.

The Dependence of ε/τ on Ultrasound Parameters

In Fig. 5 the ε/τ values are plotted as a function of skin resistivity and are calculated from Eq. (9) as follows: For each value of R, corresponding value of Δx was obtained from Fig. 4B. The values of Δx and P_p, were substituted in Eq. (9) to obtain ε/τ for each R value. In Fig. 5 data points for ultrasound application (○), passive delivery (●), and dermis (■) can be represented by a single function. The average ε/τ value for passive diffusion is ~3.5×10^{-6} and with the application of ultrasound the ε/τ value could be increased up to ~6.0×10^{-3} an enhancement of approximately 1700-fold. The ε/τ value does not directly tell if the actual porosity, ε, is increased or the tortuosity, τ, is decreased or both. Still a limiting case could be applied by assuming $C = 1$. Also, as the effect of ultrasound on skin is heterogeneous (Fig. 3) a fair assumption would be that the porosity and permeability increase mainly within the LTPs. With these assumptions and the fact that LTPs occupy approximately 5% of the sonicated skin area

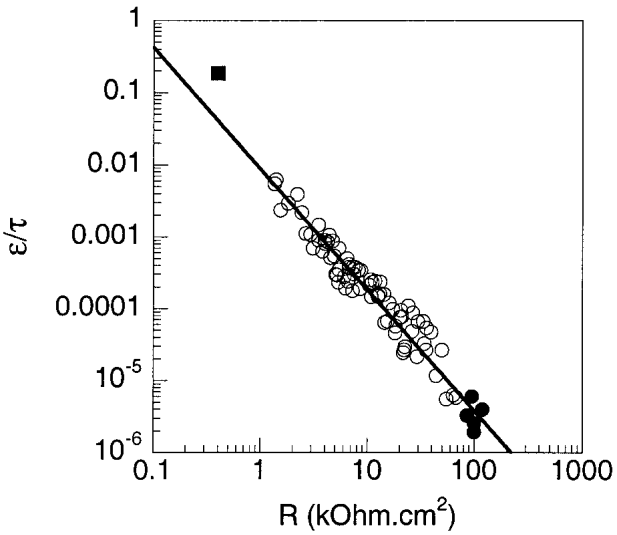

Fig. 5. The ε/τ value as a function of skin resistivity ((○)-ultrasound, (■)-dermis, (●)-passive delivery) . The line corresponds to a power fit to the data ($r^2 = 0.95$).

(quantified with Adobe Photoshop) the porosity within these areas could be calculated to be approximately 12%. Using the porous pathway model (Eq. (9)) and experimentally measured dermis permeability the dermis porosity, was calculated to be 17%. These values suggest that with the application of ultrasound, the SC barrier properties are reduced and LTPs that are on the order of magnitude as porous as the dermis are created. These results also validate the assumption that we adapted earlier in our analysis stating that the membrane thickness, Δx, should be chosen as the total affected depth rather than the SC thickness.

CONCLUSIONS

The aim of this study was to investigate the dependence of effective pore size, skin porosity, and skin tortuosity on ultrasound parameters (i.e., frequency and energy density) with the application of LFS. Porous pathway model was applied to investigate these parameters in the presence and absence of ultrasound. Both in the presence and absence of ultrasound the average pore size for mannitol delivery is the same (28 ± 12 Å). Further studies are needed to investigate why there is no frequency dependence of the effective pore size. Because the average pore size is unaffected by ultrasound application, (i.e., $H(\lambda_p) \approx$ constant) the increased skin permeability of hydrophilic permeants must be explained by increased porosity and/or decreased tortuosity (i.e., increased ε/τ ratio). With the application of ultrasound the ε/τ value could be increased up to 1700-fold compared to untreated skin (no ultrasound).

The effects of ultrasound on skin are heterogeneous create localized transport pathways. The dependence of the depth of LTPs on ultrasound frequency and skin resistivity was also studied. Again no frequency dependence was observed and the depth of transport regions created by ultrasound depended only on the skin resistivity. The porous pathway model was used to calculate the porosity of dermis and LTPs. The porosity of the LTPs was calculated to be of the same order of magnitude as the dermis.

ACKNOWLEDGMENTS

This work was supported by Centers for Disease Control and Prevention and a grant from Juvenile Diabetes Foundations. Ashley Sens acknowledges the support from the RISE fellowship from Materials Research Laboratory (MRL). The authors also thank Hua Tang for discussions on the hindered transport theory.

REFERENCES

1. G. A. Simon and H. I. Maibach. The pig as an experimental animal model of percutaneous permeation in man: qualitative and quantitative observations—an overview. *Skin Pharmacol. Appl. Skin Physiol.* **13**:229–234 (2000).
2. P. M. Elias. Epidermal lipids, barrier function, and desquamation. *J. Invest. Dermatol.* **80**:44–49 (1983).
3. T. M. Suhonen, J. A. Bouwstra, and A. Urtti. Chemical enhancement of percutaneous absorption in relation to stratum corneum structural alteration. *J. Control. Release* **59**:149–161 (1999).
4. B. Forslind, S. Engstrom, J. Engblom, and L. Norlen. A novel approach to the understanding of human barrier function. *J. Dermatol. Sci.* **14**:115–125 (1997).
5. K. A. Walters and J. Hadgraft. *Pharmaceutical Skin Penetration Enhancement*, Marcel Dekker, New York, 1993.
6. R. B. Walker and E. W. Smith. The role of percutaneous penetration enhancers. *Adv. Drug Deliv. Rev.* **18**:295–301 (1996).
7. Y. N. Kalia and R. H. Guy. Interaction between penetration enhancers and iontophoresis: Effect on human skin impedance in vivo. *J. Control. Release* **44**:33–42 (1997).
8. M. R. Prausnitz, V. Bose, R. Langer, and J. C. Weaver. Electroporation of mammalian skin: A mechanism to enhance transdermal drug delivery. *Proc. Natl. Acad. Sci. USA* **90**:10504–10508 (1993).
9. D. Levy, J. Kost, Y. Meshulam, and R. Langer. Effect of ultrasound on transdermal drug delivery to rats and guinea pigs. *J. Clin. Invest.* **83**:2974–2978 (1989).
10. S. Mitragotri, D. Blankschtein, and R. Langer. Transdermal drug delivery using low frequency sonophoresis. *Pharm. Res*. **13**:411–420 (1996).
11. S. Mitragotri, D. Blankschtein, and R. Langer. Ultrasound-mediated transdermal protein delivery. *Science* **269**:850–853 (1995).
12. W. Gaertner. Frequency dependence of acoustic cavitation. *J. Acoust. Soc. Am.* **26**:977–980 (1954).
13. A. Tezel, A. Sens, J. Tuchscherer, and S. Mitragotri. Frequency dependence of sonophoresis. *Pharm. Res.* **18**:1694–1700 (2001).
14. H. Tang, S. Mitragotri, D. Blankschtein, and R. Langer. Theoretical description of transdermal transport of hydrophilic permeants: Application to low-frequency sonophoresis. *J. Pharm. Sci.* **90**:545–568 (2001).
15. S. K. Li, A. H. Ghanem, K. D. Peck, and W. I. Higuchi. Pore induction in human epidermal membrane during low to moderate voltage iontophoresis: A study using AC iontophoresis. *J. Pharm. Sci.* **88**:419–427 (1999).
16. M. Sznitowska, S. Janicki, and A. C. Williams. Intracellular or intercellular localization of the polar pathway of penetration across stratum corneum. *J. Pharm. Sci.* **87**:1109–1114 (1998).
17. G. Cevec and H. Richardsen. Lipid vesicles and membrane fusion. *Adv. Drug Deliv. Rev.* **38**:207–232 (1999).
18. W. M. Deen. Hindered transport of large molecules in liquid-filled pores. *AIChE.* **33**:1409–1424 (1987).
19. S. Mitragotri, D. Ray, J. Farrell, H. Tang, B. Yu, J. Kost, D. Blankschtein, and R. Langer. Synergistic effect of Low-Frequency Ultrasound and Sodium Lauryl Sulfate on Transdermal Transport. *J. Pharm. Sci.* **89**:892–900 (2000).
20. A. Tezel, A. Sens, J. Tuchscherer, and S. Mitragotri. Synergistic effect of low frequency ultrasound and surfactants on skin permeability. *J. Pharm. Sci.* **91**:91–100 (2002).